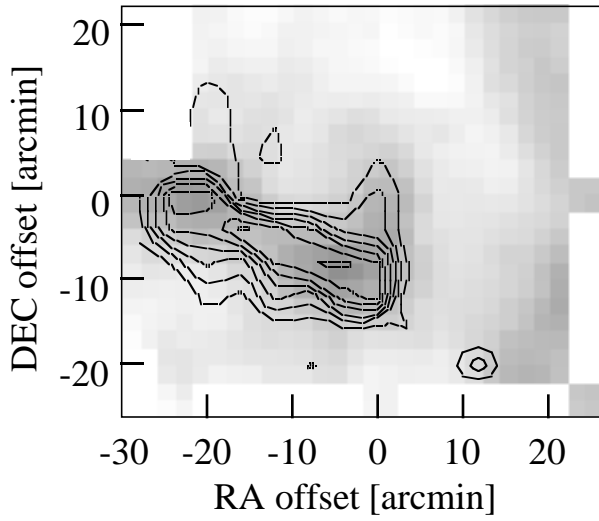
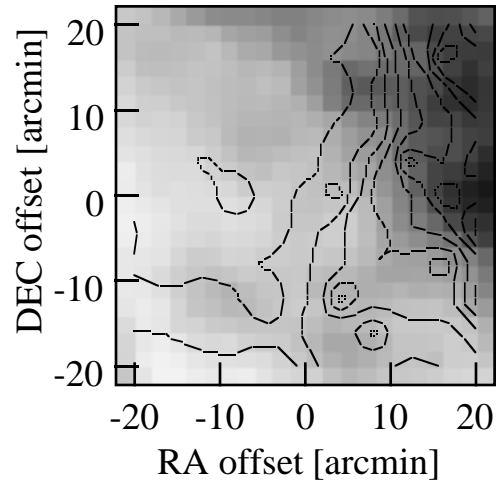


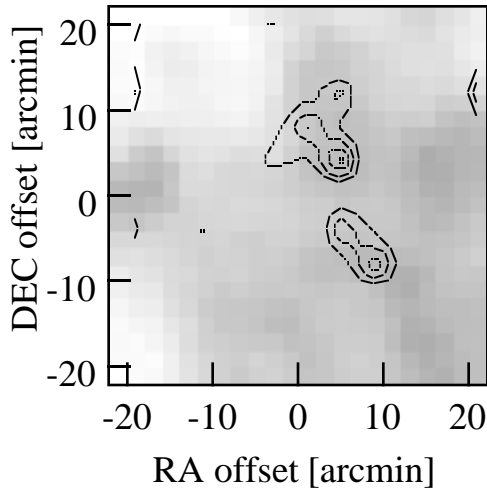
(a) Beam Position 3



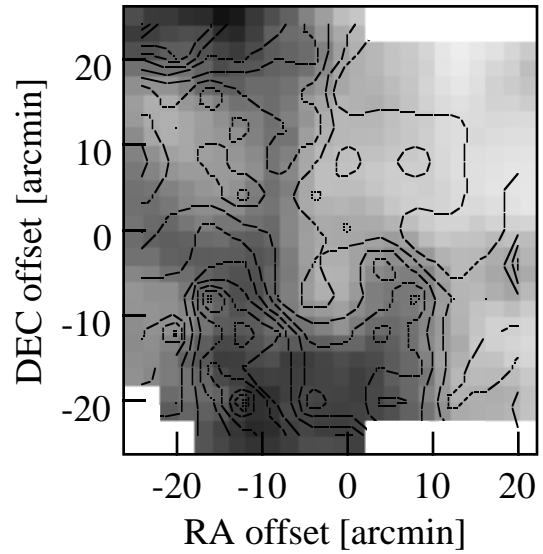
(d) Beam Position 8



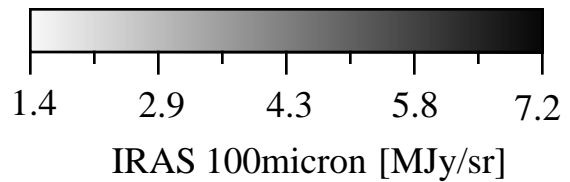
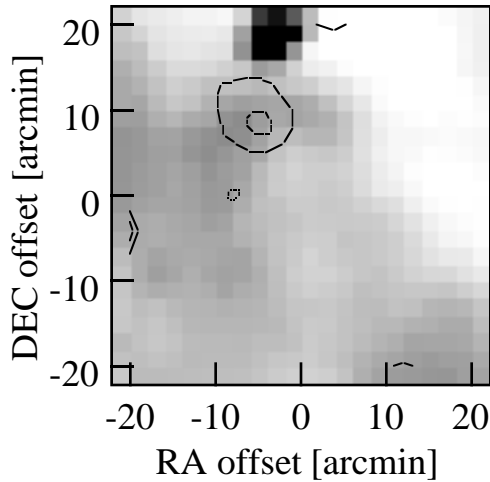
(b) Beam Position 4

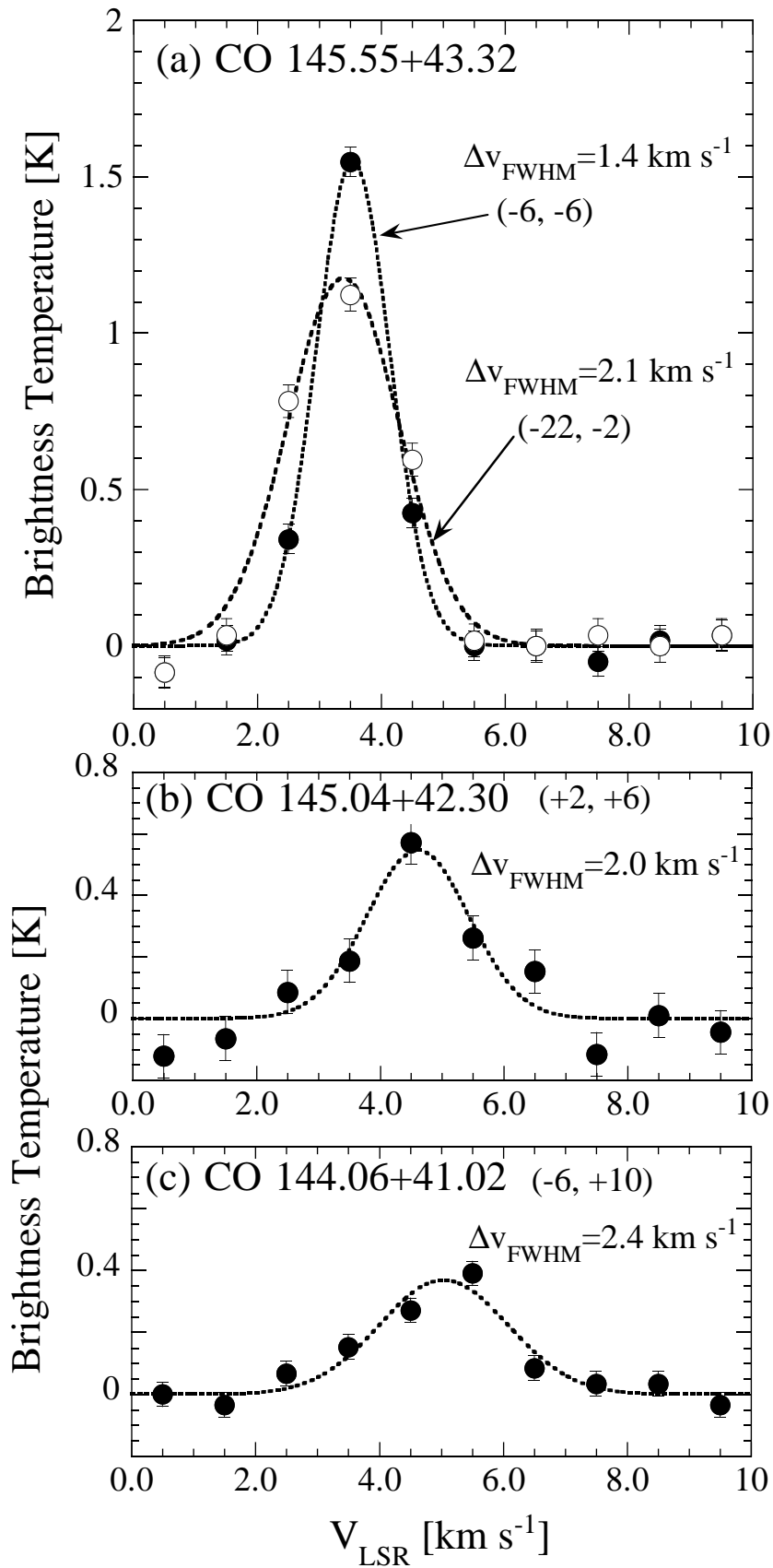


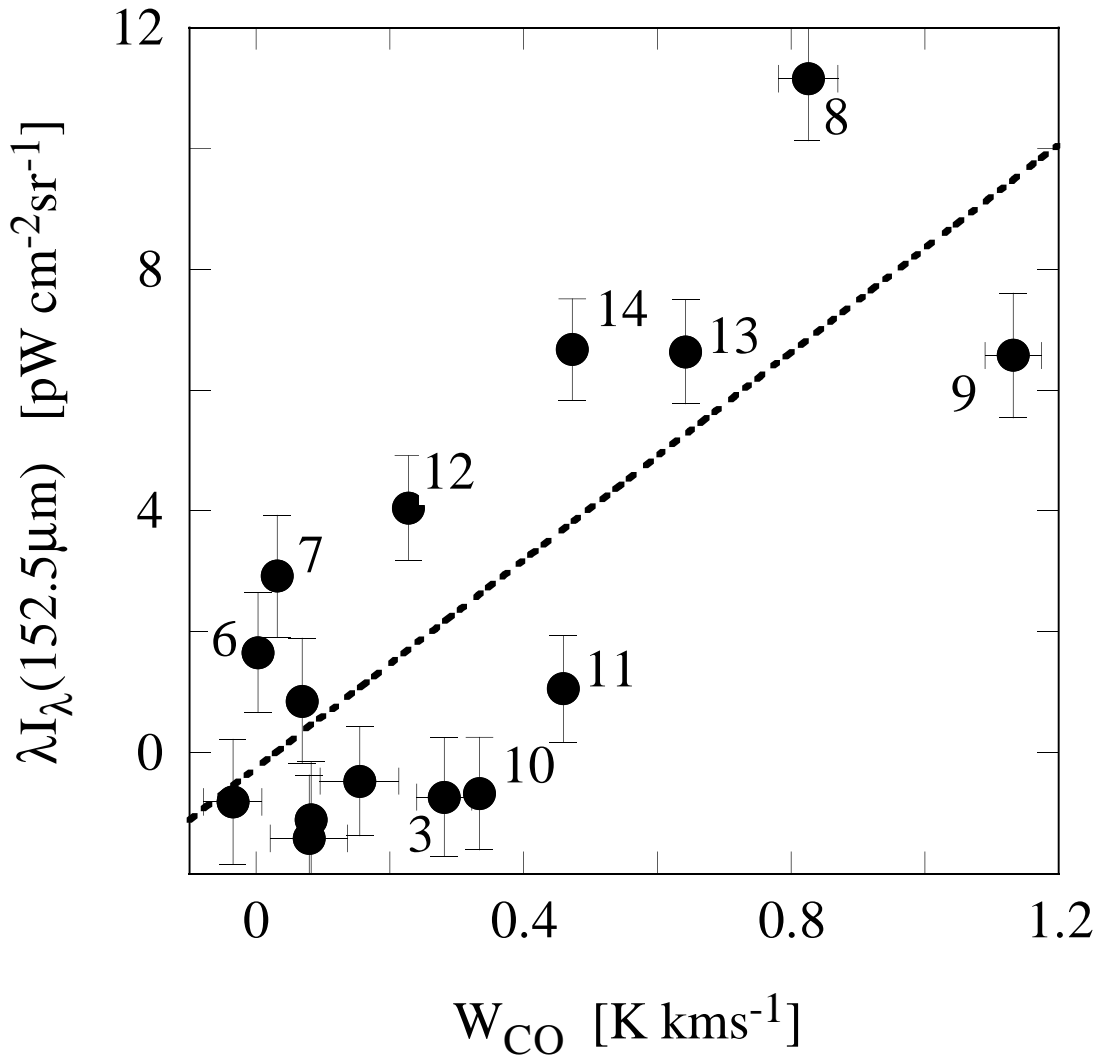
(e) Beam Position 9



(c) Beam Position 5







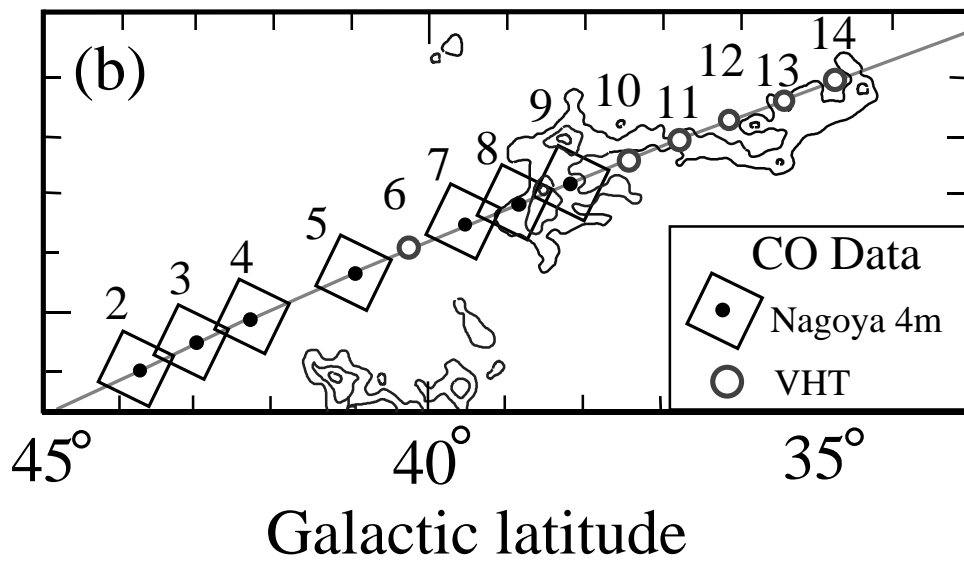
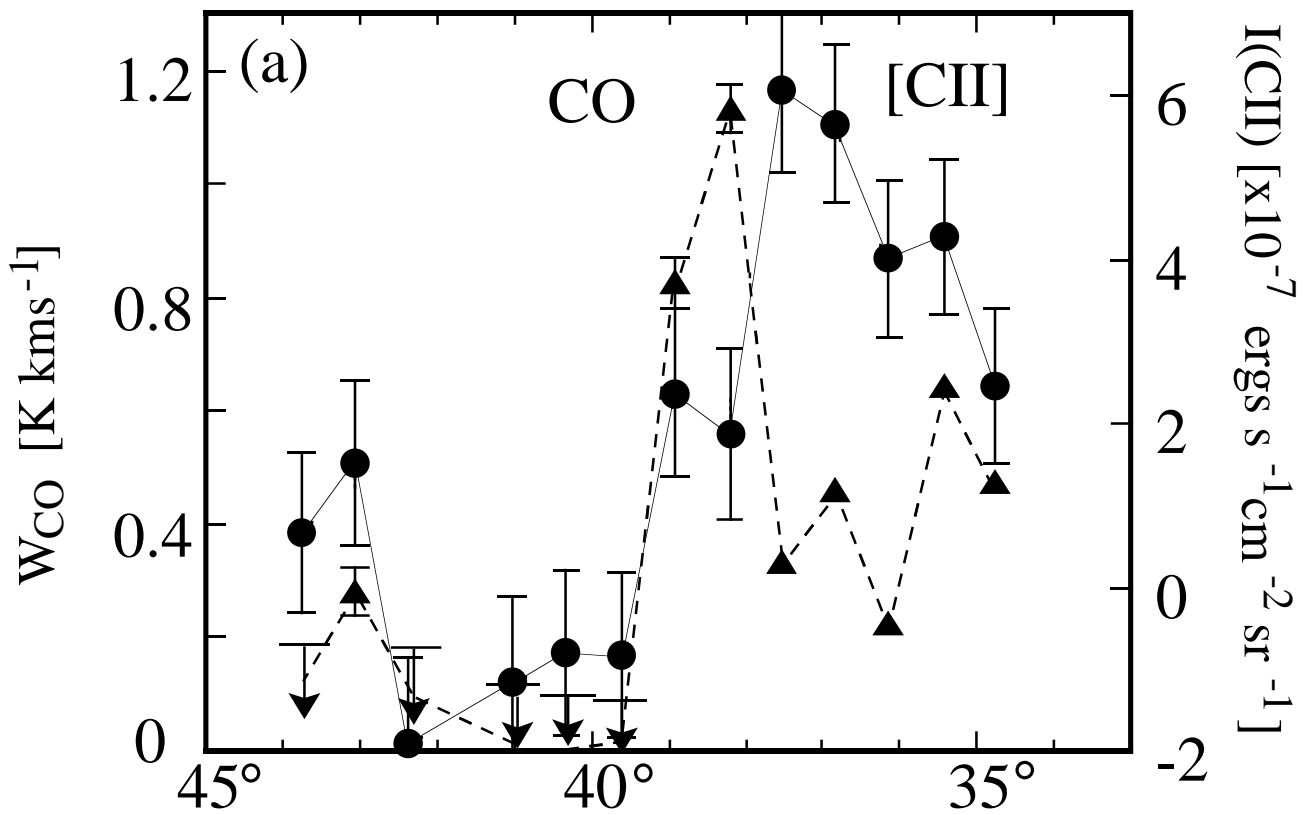


TABLE 1  
SPECIFICATIONS OF THE SPECTROPHOTOMETER

Channel Name	CC	LC
$\lambda_{peak}$ [ $\mu\text{m}$ ] <sup>a</sup>	152.43	157.66
$\lambda_C$ [ $\mu\text{m}$ ] <sup>b</sup>	152.54	157.75
$\lambda_C/\Delta\lambda$ <sup>b</sup>	89.7	100.0
Beam(FWHM) [']	36	36

<sup>a</sup> Wavelengths at peak responses.

<sup>b</sup> Effective band center wavelength( $\lambda_C$ ) and equivalent square band width for  $I_\nu \propto \nu^{-0.5}$  ( $\Delta\lambda$ ).

TABLE 2  
 PROPERTIES OF THE MOLECULAR CLOUDS

Cloud	$\alpha(1950)$	$\delta(1950)$	$\Delta v$ <sup>a</sup> [km s <sup>-1</sup> ]	size(A) [deg <sup>2</sup> ]	R <sup>b</sup> [pc]	Mass <sup>c</sup> [ $M_{\odot}$ ]	$n(H_2)$ <sup>d</sup> [cm <sup>-3</sup> ]	$P_{grav}$ <sup>e</sup> [ergs cm <sup>-3</sup> ]	$P_{turb}$ <sup>f</sup> [ergs cm <sup>-3</sup> ]
CO 145.55+43.32	9h57.2m	65°49'	2.1	0.10	0.31	1.7	$2 \times 10^2$	$4.2 \times 10^{-14}$	$7.2 \times 10^{-12}$
CO 145.04+42.30	9h50.8m	66°42'	2.0	0.009	0.10	0.27	$1 \times 10^3$	$1.4 \times 10^{-13}$	$3.8 \times 10^{-11}$
CO 144.06+41.02	9h43.6m	67°59'	2.4	0.018	0.13	0.094	$1 \times 10^2$	$4.1 \times 10^{-15}$	$6.9 \times 10^{-12}$
MBM clouds <sup>g</sup>	9h23.7m	69°57'	2.9	3.8	1.9	32.4 <sup>h</sup>	20	$1.4 \times 10^{-14}$	$2.5 \times 10^{-12}$

<sup>a</sup> Typical observed line widths(in FWHM) of the CO emission.

<sup>b</sup> Calculated by  $R = (A/\pi)^{1/2} * D$ , where  $A$  is area of the emission region, and  $D$  is the distance to the source (assuming  $D=100$ pc).

<sup>c</sup> Calculated by using  $X \equiv N(H_2)/W_{CO} = 1.2 \times 10^{20} \text{ cm}^{-2} (\text{K km s}^{-1})^{-1}$ , mean molecular weight=1.4, and  $D = 100$ pc.

<sup>d</sup> Average volume density of molecular hydrogen assuming the spherical volume of radius  $R$ .

<sup>e</sup> Gravitation pressure at radius  $R$ .

<sup>f</sup> Pressure at radius  $R$  due to turbulent gas motion in the cloud(calculated from the velocity width).

<sup>g</sup> MBM 27/28/29/30 = "CO 1" in Table 1 of VHT.

<sup>h</sup> Value in VHT is  $13.3M_{\odot}$ , using  $X = 0.5 \times 10^{20} \text{ cm}^{-2} (\text{K km s}^{-1})^{-1}$ .



to appear in ApJ Vol.490, December 1, 1997 issue

## Observations of [C II] 158 micron Line and Far-infrared Continuum Emission toward the High-latitude Molecular Clouds in Ursa Major

Hideo Matsuhara, Masahiro Tanaka<sup>1</sup>, Yoshinori Yonekura, and Yasuo Fukui

Department of Astrophysics, Nagoya University, Furo-cho, Chikusa-ku, Nagoya 464-01,  
Japan;

maruma@toyo.phys.nagoya-u.ac.jp, tanaka@toyo.phys.nagoya-u.ac.jp,  
yonekura@a.phys.nagoya-u.ac.jp, fukui@a.phys.nagoya-u.ac.jp

Mitsunobu Kawada

the Institute of Space and Astronautical Science, 3-1-1 Yoshinodai, Sagamihara, Kanagawa  
229, Japan;

kawada@koala.astro.isas.ac.jp

and

James. J. Bock

Observational Cosmology, California Institute for Technology, 1201 E. California Blvd.,  
Pasadena, CA 91125;

jjb@astro.caltech.edu

### ABSTRACT

We report the results of a rocket-borne observation of [C II] 158 $\mu$ m line and far-infrared continuum emission at 152.5 $\mu$ m toward the high latitude molecular clouds in Ursa Major. We also present the results of a follow-up observation of the millimeter <sup>12</sup>CO  $J = 1 \rightarrow 0$  line over a selected region observed by the rocket-borne experiment. We have discovered three small CO cloudlets from the follow-up <sup>12</sup>CO observations. We show that these molecular cloudlets, as well as the MBM clouds (MBM 27/28/29/30), are not gravitationally bound. Magnetic pressure and turbulent pressure dominate the dynamic balance of the clouds.

---

<sup>1</sup>present address: the Institute of Space and Astronautical Science, 3-1-1 Yoshinodai, Sagamihara, Kanagawa 229, Japan; masa@koala.astro.isas.ac.jp

After removing the HI-correlated and background contributions, we find that the [C II] emission peak is displaced from the  $152.5\mu\text{m}$  and CO peaks, while the  $152.5\mu\text{m}$  continuum emission is spatially correlated with the CO emission. We interpret this behavior by attributing the origin of [C II] emission to the photodissociation regions around the molecular clouds illuminated by the local UV radiation field. We also find that the ratio of the molecular hydrogen column density to velocity-integrated CO intensity is  $1.19 \pm 0.29 \times 10^{20} \text{ cm}^{-2} (\text{K km s}^{-1})^{-1}$  from the FIR continuum and the CO data. The average [C II] /FIR intensity ratio over the MBM clouds is 0.0071, which is close to the all sky average of 0.0082 reported by the FIRAS on the COBE satellite. The average [C II]/CO ratio over the same regions is 420, which is significantly lower than that of molecular clouds in the Galactic plane.

*Subject headings:* general–infrared: general–ISM: interstellar

## 1. Introduction

The [C II] ( $^2P_{3/2} \rightarrow ^2P_{1/2}$ )  $157.7\mu\text{m}$  line emission is thought to be an important coolant of the diffuse interstellar medium (Dalgarno & McCray 1972; Spitzer 1978). In recent theoretical studies the [C II] line dominates the cooling of the cold neutral medium (Wolfire et al. 1995), and low density photodissociation regions (PDRs) around the surface of molecular clouds (Hollenbach, Takahashi, & Tielens 1991). The PDR models (Tielens & Hollenbach 1985; Hollenbach et al. 1991) are in agreement with observations of [C II] emission from individual star forming regions at the edge of the molecular clouds and the diffuse [C II] emission from the Galactic plane (Shibai et al. 1991; Wright et al. 1991). Observation of [C II] emission from PDRs, however, has been limited to regions with  $G_0 > 10$ , where  $G_0$  is the far-ultraviolet (FUV) field strength normalized to Habing’s (1968) estimate of the local interstellar flux, due to the low brightness of [C II] emission from PDRs with  $G_0$  as small as that found locally. Observation of local high latitude molecular clouds thus provides a unique example for study of such PDRs. The high latitude molecular clouds studied in this paper are believed to be located in the solar neighborhood (Magnani, Blitz, & Mundy 1985, hereafter MBM).

Observation of diffuse [C II] line emission at high Galactic latitude is, however, only possible from space due to the low brightness of the line from these regions. Balloon-borne and air-borne observations do not have enough sensitivity because of the enormous background from the earth’s atmosphere and from the ambient temperature telescope. The

FIRAS onboard the COBE satellite has observed the [C II] line over almost the entire sky with a  $7^\circ$  beam (Wright et al. 1991; Bennett et al. 1994), which is however too large to observe [C II] emission from high latitude molecular clouds.

In February 1992 we made a rocket-borne observation of [C II]  $158\mu\text{m}$  line and far-infrared(FIR) continuum emission of a region at high Galactic latitude in Ursa Major with higher sensitivity and higher angular resolution ( $0.6^\circ$ ) than those of the COBE/FIRAS. Details of the experiment are described in Matsuhara et al. (1994). The correlation of the [C II] line with atomic hydrogen(HI) column density in regions without appreciable CO emission has already been reported by Bock et al. (1993). The FIR continuum observations of both atomic and molecular regions have been presented by Kawada et al. (1994).

The main purpose of this paper is to present the first observation of the [C II] line from high latitude molecular clouds. We also report the results of a follow-up observation of the millimeter  $^{12}\text{CO J}=1\rightarrow 0$  line with a 4m millimeter telescope at Nagoya university. The rocket-borne observations pass over high latitude molecular clouds studied by MBM: MBM 27/28/29/30.  $^{12}\text{CO}$  emission from these high latitude clouds (hereafter MBM clouds) has already been well studied by de Vries, Heithausen, & Thaddeus (1987, hereafter VHT). In previous works (Bock et al. 1993; Kawada et al. 1994) we implicitly assumed there are no molecular regions except for those reported by VHT. The follow-up CO observation enables us to check the validity of this assumption. In this paper we assume the distance to the Ursa Major clouds is  $D=100\text{pc}$ , as adopted by VHT. Penprase (1993) constrained the distance of the clouds by optical absorption line observations toward bright stars with known distances:  $100\text{pc} < D < 120\text{pc}$ .

In the following we describe the rocket-borne observation and the results (§2), the millimeter CO observation and the results (§3), and then discuss the physical properties of the molecular clouds and the origin of the [C II] emission from the MBM clouds (§4).

## 2. Rocket-borne Observation and Results

### 2.1. Observation

The rocket-borne instrument consists of an absolute 2-channel spectrophotometer at the focus of 10cm liquid-helium cooled telescope which measures [C II]  $157.7\mu\text{m}$  velocity-integrated flux (LC channel) and nearby continuum flux at  $152.5\mu\text{m}$  (CC channel)

simultaneously. Specifications of the spectrophotometer are summarized in Table 1<sup>2</sup>. Details of the instrument and the method of the [C II] observation may be found in Matsuhara et al. (1994) and Bock et al. (1993), respectively.

The instrument was integrated with the sounding rocket S-520-15 of the institute of Space and Astronautical Science (ISAS) in Japan and launched on 1992 February 2 from the Kagoshima Space Center of the ISAS. Observations began at 130s after launch when a lid covering the telescope was opened, and ended at 480s when the instrument was separated from the rocket payload.

Observed regions are shown in Figure 1. For more than half of the observation time the telescope was pointed at the HI hole,  $(l, b) \sim (151^\circ, 52^\circ)$ . From 220s to 310s after launch, the telescope scanned along a triangular path as shown in Figure 1, through the high latitude molecular clouds (MBM clouds) and over the FIR bright galaxy M82, which was observed for in-flight calibration of the instrument.

## 2.2. Results

The data used in this paper are the LC and CC data obtained between 222 and 357s after launch, during which the triangular scanning observation and a part of the second pointed observation of the HI hole were made. The laboratory calibration of the sensitivity, the in-flight subtraction of the instrumental offset, and the in-flight response calibration are described in Bock et al. (1993) and Kawada et al. (1994). The response of the spectrophotometer was monitored by an internal calibration lamp in flight, and was closely matched with the response observed in the laboratory. We estimate the uncertainty of the absolute brightness calibration is 6.4% for 152.5 $\mu$ m continuum, and 8.4% for the [C II] line.

As described in Bock et al., the [C II] line intensity is extracted from the difference of LC signal and CC signal. Thus the derived [C II] intensity depends on the spectral index  $s$  ( $I_\nu \propto \nu^s$ ) of the continuum between 152 and 158 $\mu$ m, and we previously assumed  $s = -1$ . In Kawada et al. (1994), we reported the FIR continuum spectra of the observed regions using the broad-band photometer data. We derive  $s = -0.25$  for the spectrum at the HI hole and  $s = -0.65$  for the spectrum of a bright IR cirrus. We find that in the worst case the assumption  $s = -1$  leads to 10% systematic error in the [C II] intensity, so in this

---

<sup>2</sup>As a result of careful analysis of the spectral response of the spectrophotometer, the effective band center wavelength and the equivalent square band width listed in Table 1 have been slightly corrected from those in Table 2 of Matsuhara et al. (1994) and in Table 1 of Kawada et al. (1994). The differences are very small and do not affect any scientific results of previously published papers.

paper we use  $s = -0.5$ . The statistical error is derived from the data obtained during the pointed observation of the HI hole between 310s and 357s after launch as in Kawada et al.:  $0.7\text{pWcm}^{-2}\text{sr}^{-1}$  for CC,  $0.8\text{pWcm}^{-2}\text{sr}^{-1}$  for LC, respectively. The  $3\sigma$  [CII] line detection limit is estimated to be  $2.7 \times 10^{-7} \text{ergs s}^{-1}\text{cm}^{-2}\text{sr}^{-1}$ .

We compare the resulting [C II] and  $152.5\mu\text{m}$  continuum data with the HI data(Heiles 1992, private communication) and the CO data of VHT. After Bock et al. was published, we determined the positions of the telescope more accurately( $\pm 3'$ ) using the near-infrared spectrometer data(Matsuura et al. 1994; Matsuhara et al. 1994). We find that the assumed pointing data used in Bock et al. were systematically offset by  $\sim 8'$ , so we re-sampled the HI data and the CO data as we did in Kawada et al. The pointing correction is significant for the CO data, since the size of the CO clouds is generally smaller than the  $36'$  beam.

The molecular clouds coincide with HI clouds emitting comparable [C II] line and FIR continuum. Hence in order to determine the [C II] and FIR continuum intensities emitted from the molecular clouds alone, we have to estimate the contributions from the HI and background components to the observed [C II] and continuum emission. As shown in §3.2, appreciable CO emission is found only for beams with  $N_{\text{HI}} > 2 \times 10^{20}\text{cm}^{-2}$ . Thus we assume that all data with  $N_{\text{HI}} < 2 \times 10^{20}\text{cm}^{-2}$  do not have appreciable CO emission, and bin these  $N_{\text{HI}}$  data in  $0.1 \sim 0.2 \times 10^{20}\text{cm}^{-2}$  intervals. Several beams(1, 2, 4, 5, 6, 7, 15, 16) are also denoted which have  $N_{\text{HI}} > 2 \times 10^{20}\text{cm}^{-2}$  but lack appreciable CO emission. The results are shown in Figure 2.

### 3. Millimeter $^{12}\text{CO}$ Observation and Results

#### 3.1. Observation

We use the millimeter-wave  $^{12}\text{CO}$  emission data to distinguish regions with significant molecular hydrogen. However, the beam positions of the rocket-borne instrument are not fully mapped by VHT. Thus, in order to increase the number of beams with  $^{12}\text{CO}$  data, we have observed at eight beam positions along the rocket observation path(labeled in Figure 1) with the Nagoya University 4m millimeter telescope(Fukui & Sakakibara 1992) in 1994 February – March. Among them, beams 7, 8 and 9 were also mapped by VHT.

Because the beam of the rocket observation( $36'$  in diameter) is much larger than that of millimeter CO observation( $2'.7$ ), we mapped at each beam position over a  $40' \times 40'$  or wider area. The mapping grid sizes were  $4' - 5'.66$ , except for parts of beams 5, 8, 9 where a further  $5 \times 5$  map was made around the emission peak with a  $2'$  grid. Integration time per each grid point was 3 – 6min with typical rms noise of 0.3K per spectral channel( $0.1\text{km s}^{-1}$ ).

We used a frequency switching method to obtain the line signal without observing a spatial reference point. Typically data at  $v < -4\text{km s}^{-1}$  and  $v > 10\text{km s}^{-1}$  are used as the baseline for the  $^{12}\text{CO}$  line spectrum. We frequently observed Orion A for brightness calibration, and assumed its brightness temperature is 60K. We also frequently observed the peak brightness position in beam 9 to correct the effect of varying airmass, which we found to be negligible.

### 3.2. Results

We obtained a positive CO detection in 5 beams(3, 4, 5, 8, and 9), all of which have relatively large  $N_{\text{HI}}(> 2 \times 10^{20}\text{cm}^{-2})$ . Contour maps of the velocity-integrated brightness temperature of the CO line( $W_{\text{CO}}$ , in  $\text{K km s}^{-1}$ ) of these beams are shown in Figure 3, superposed on  $100\mu\text{m}$  maps reproduced from the IRAS Sky Survey Atlas(ISSA) by reducing the intensity by a factor of 0.72, following the COBE/DIRBE calibration (Wheelock et al. 1994). The spatial distribution of the integrated CO line in beams 8 and 9(Figs. 3d and 3e) are in good agreement with those of VHT. However, we find that the absolute brightness temperature of VHT is systematically lower by a factor of 0.68. Since the purpose of the CO observation in this work is to supplement the observation of VHT, we scaled the brightness temperature of all data so that our data of beams 8 and 9 match the data of VHT.

We discovered a few isolated, small CO cloudlets in beams 3, 4, 5. The typical spectra of the CO cloudlets are shown in Figure 4. The spectral data are integrated in  $1\text{km s}^{-1}$  bins and fitted by a gaussian in order to evaluate the line widths. Location, size, line width, and the derived physical properties(details are described in §4.3) of the cloudlets are listed in Table 2.

In order to compare with the rocket-borne data, average  $W_{\text{CO}}$  was calculated by convolving the CO data with the  $36'$  beam of the rocket-borne instrument. Although we have a positive CO detection in beams 4 and 5, these cloudlets are very small compared with the rocket beam and thus when averaged over the  $36'$  beam do not give appreciable average  $W_{\text{CO}}$ (more than  $3\sigma$ :  $\sim 0.2\text{K km s}^{-1}$ ) for these beams. In the averaging procedure the error is dominated by the poor quality of the spectral baselines incurred at some grid positions due to temporal changes of the weather condition during the observation. Only for beams 3, 8, and 9 did we obtain appreciable  $W_{\text{CO}}(> 0.2\text{K km s}^{-1})$ .

## 4. Discussion

#### 4.1. HI regions

In previously published papers (Bock et al. 1993; Kawada et al. 1994), we assumed that there are no molecular regions except for those mapped by VHT. Outside the regions mapped by VHT, only beam 3 has appreciable CO emission. Therefore, the previous results on the physical properties of the HI regions do not change significantly. We summarize the results for the HI regions for purposes of the following analysis of the molecular regions.

The correlation between  $152.5\mu\text{m}$  continuum emission and HI column density is shown in Figure 2a, and the correlation between [C II] emission and HI column density is shown in Figure 2b. The excellent correlation of the  $152.5\mu\text{m}$  continuum intensity and HI column density strongly suggests that instrumental effects such as detector hysteresis are small. Laboratory data demonstrate that detector hysteresis is still further removed in the [C II] profile which is derived by difference of signals between two well-matched detectors.

The  $152.5\mu\text{m}$  continuum emissivity per HI column density is determined to be  $\lambda I_\lambda/N_{\text{HI}} = 3.62 \pm 0.38 \times 10^{-32} \text{ W sr}^{-1}$ , and the [C II] cooling rate per atomic hydrogen is determined to be  $\Lambda_{\text{CII}} \equiv 4\pi I(\text{C II})/N_{\text{HI}} = 1.32 \pm 0.24 \times 10^{-26} \text{ ergs s}^{-1} \text{ H}_{\text{atom}}^{-1}$ . This value is in good agreement with the average cooling rate at high latitude obtained by recent analysis of the COBE/FIRAS data:  $\Lambda_{\text{CII}} = 1.45 \times 10^{-26} \text{ ergs s}^{-1} \text{ H}_{\text{atom}}^{-1}$  (Dwek et al. 1997). If only data with  $N_{\text{HI}} < 2 \times 10^{20} \text{ cm}^{-2}$  are considered, these values change little:  $\lambda I_\lambda/N_{\text{HI}} = 2.66 \pm 0.45 \times 10^{-32} \text{ W sr}^{-1}$ ,  $\Lambda_{\text{CII}} = 1.64 \pm 0.39 \times 10^{-26} \text{ ergs s}^{-1} \text{ H}_{\text{atom}}^{-1}$ . As already noted by Bock et al., inclusion of the region with relatively low line-to-continuum ratio (beams 4, 5, 6, and 7) tends to increase the FIR continuum emissivity and to decrease the [C II] line cooling rate. These uncertainties in  $\lambda I_\lambda/N_{\text{HI}}$  and  $\Lambda_{\text{CII}}$  of the HI correlated components are, however, not significant in deriving the intensity of [C II] line and FIR continuum from the molecular regions, and thus do not appreciably affect the following discussion.

#### 4.2. The Conversion Factor $X = N(\text{H}_2)/W_{\text{CO}}$

We subtract the HI and background contributions from the  $152.5\mu\text{m}$  continuum and obtain the excess FIR emission plotted against  $W_{\text{CO}}$  in Figure 5. The fitted line in Figure 5 gives  $\lambda I_\lambda/W_{\text{CO}} = 8.6 \pm 2.1 \text{ pW cm}^{-2} \text{ sr}^{-1} (\text{K km s}^{-1})^{-1}$  with no significant residual FIR emission at  $W_{\text{CO}} = 0$ . The conversion factor  $X \equiv N(\text{H}_2)/W_{\text{CO}}$ , the parameter used to estimate the molecular column density over CO clouds, is derived assuming constant FIR emissivity per hydrogen nucleus in both the molecular and the HI regions. We find  $X = 1.19 \pm 0.29 \times 10^{20} \text{ cm}^{-2} (\text{K km s}^{-1})^{-1}$ , which is not significantly different from the value

derived by Kawada et al. (1994).

The conversion factor  $X$  is presumably not constant, varying significantly from region to region. VHT gives  $X = 0.5 \pm 0.3 \times 10^{20} \text{ cm}^{-2} (\text{K km s}^{-1})^{-1}$  over a larger region of the molecular clouds using IRAS  $100\mu\text{m}$  data. We independently examine the factor  $X$  on small scales by studying the correlation between CO and IRAS  $100\mu\text{m}$  emission for beams 3, 8, and 9 where CO counterparts are clearly visible in the IRAS  $100\mu\text{m}$  maps (Fig. 3). No correction for the HI component is applied to the IRAS  $100\mu\text{m}$  data, so significant spatial structure in HI column density invalidates this analysis. From the slopes of the fitted lines and the global FIR spectrum of dust emission ( $\lambda I_\lambda(152.5\mu\text{m})/\lambda I_\lambda(100\mu\text{m}) = 1.5(+0.4, -0.3)$ ; Kawada et al.), we derive the factor  $X$  for beams 3, 8, 9 as  $0.54(+0.27, -0.24)$ ,  $1.0(+0.43, -0.36)$ ,  $0.86(+0.41, -0.35) \times 10^{20} \text{ cm}^{-2} (\text{K km s}^{-1})^{-1}$ , respectively. While the factor  $X$  for beams 8 and 9 is consistent with the global value, that of beam 3 is appreciably lower.

### 4.3. Physical Properties of the Molecular Clouds

In Table 2 the mass of the clouds calculated from the integrated CO flux and the (global) conversion factor  $X$  are listed. The distance to the clouds is not known for the small cloudlets in beams 3, 4, and 5, and thus the mass of these cloudlets is calculated by assuming the same distance of that of the MBM clouds:  $D = 100\text{pc}$ . In addition, considering the local variation of the factor  $X$  as described in the previous subsection, the mass of the cloudlets may be smaller by a factor of 2.

The average volume density of molecular hydrogen, calculated by assuming a spherical cloud of radius  $R$  ( $= (A/\pi)^{1/2} * D$ , where  $A$  is solid angle of the cloud), is also shown in Table 2. For the MBM clouds, the assumption of a spherical geometry is clearly not applicable. However, the average density derived by dividing the column density of molecular hydrogen by the width of the CO filament ( $\sim 1\text{pc}$  in the plane of sky) ranges from  $10 - 50\text{cm}^{-3}$ , similar value to that calculated by assuming a spherical cloud. It is interesting that the density of the small cloudlets in beams 3, 4, and 5 is much larger than that of the MBM clouds. This may suggest that the MBM clouds are very clumpy, consisting of smaller, denser cloudlets like those in beams 3, 4, and 5. Another interesting fact is that the average number density of these clouds is too low for CO molecules to survive photodissociation rate from the interstellar UV field. For example,  $n(\text{H}_2)R \sim 2 \times 10^{20} \text{ cm}^2$ , corresponding to  $A_V \simeq 0.1\text{mag}$ , for CO 145.55+43.32 (the cloudlet in beam 3). Thus, to survive the photodissociation, the clouds may consist of many small and dense clumps. In this case, since we did not observe such clumpy structure with the 4m telescope, each clump must be small enough to be unresolved ( $< 2'$ ). Alternatively, the UV photons may be



strongly attenuated by intervening clouds between the UV sources and the CO cloudlets(see §4.4).

In Table 2 rough estimates of the turbulent pressure( $P_{turb}$ ) and the gravitational pressure( $P_{grav}$ ) are listed for the cloudlets in beams 3, 4, and 5, and for the MBM clouds. The turbulent pressure of the clouds is estimated from the  $^{12}\text{CO}$  velocity width( $\Delta v_{\text{FWHM}}$ ; Fig. 4), the calculated mass  $M$  of the cloud, and the effective radius  $R$ , using  $4\pi R^2 P_{turb} = 3M\Delta v_{\text{FWHM}}^2/(8\ln 2)R$ . The gravitational pressure, calculated as  $4\pi R^2 P_{grav} = 3GM^2/5R^2$ , is orders of magnitude smaller than the turbulent pressure. Since the external thermal pressure of the HI gas(estimated by the [C II] line cooling rate, see Bock et al. (1993)),  $\sim 10^{-13}$  ergs  $\text{cm}^{-3}$ , is also much smaller than the turbulent pressure, the cloud cannot be bound by gravitation or by external thermal pressure. Joncas et al. (1992) calculated the magnetic pressure, by using the magnetic field strength at  $(l, b) = (142^\circ.6, 38^\circ.4)$  (close to beam 9) measured by Heiles (1989), to be  $1 \times 10^{-11}$  ergs  $\text{cm}^{-3}$ . Joncas et al. also estimated the turbulent pressure of the HI gas to be  $4 \times 10^{-11}$  ergs  $\text{cm}^{-3}$  from the velocity width of the HI emission line. Thus as Joncas et al. concluded for the HI clouds, the turbulent pressure in these molecular clouds is possibly balanced by the magnetic pressure as well as the external turbulent pressure of the HI gas.

#### 4.4. [C II] Emission from the MBM Clouds

In Figure 6 we compare the spatial distribution of  $W_{\text{CO}}$  and excess(*i.e.* corrected for HI and background contributions) [C II] line emission. Interestingly, the spatial distribution of the excess [C II] emission is very much different from that of  $W_{\text{CO}}$  while the  $152.5\mu\text{m}$  continuum emission is correlated with  $W_{\text{CO}}$ (Fig. 5). The [C II] emission peak is displaced from the CO peak toward lower latitude by  $\sim 1^\circ$ . In the following we discuss the origin of the excess [C II] emission and present the most plausible interpretation of this interesting behavior.

Excess [C II] emission could possibly originate from H II gas ionized by Lyman continuum photons or Galactic shock waves. Such ionized component of the local interstellar medium, the warm ionized medium(WIM), is responsible for diffuse  $\text{H}\alpha$  emission(Reynolds 1993, and references therein). However, the  $\text{H}\alpha$  intensity over the entire observed region is unusually low( $I(\text{H}\alpha) \simeq 0.7 \pm 0.5 \times 10^{-7}$  ergs  $\text{s}^{-1}\text{cm}^{-2}\text{sr}^{-1}$ ; Reynolds, private communication) compared with the average  $\text{H}\alpha$  intensity for  $|b| \leq 15^\circ$ ,  $\langle I(\text{H}\alpha) \rangle \simeq 2.9 \times 10^{-7} \text{csc } |b|$  ergs  $\text{s}^{-1}\text{cm}^{-2}\text{sr}^{-1}$ (eq. (8) of Reynolds 1992). In the low-density limit the [C II] line intensity is proportional to the emission measure and hence proportional to the  $\text{H}\alpha$  intensity,  $I(\text{C II}) \simeq 1.45I(\text{H}\alpha)$  for  $T = 10^4\text{K}$  and  $\text{C}^+/\text{H} = 3.3 \times 10^{-4}$ (eq.(6)

of Reynolds 1992). Thus we conclude that [C II] emission associated with the WIM is negligible,  $I(\text{C II}) \leq 2 \times 10^{-7} \text{ ergs s}^{-1} \text{ cm}^{-2} \text{ sr}^{-1}$ .

The excess [C II] emission may originate from shock-compressed HI gas since the MBM clouds are located in the north celestial loop, a large ( $\sim 20^\circ$ ) loop of HI gas produced by stellar winds or supernovae explosions (Heiles & Habing 1974). Since [C II] emission is a collisionally excited line, emission from the shock-compressed (or shock-heated) HI gas is stronger than that of ambient low-density HI gas. In order to explain the observed [C II] strength of the beams 10 – 14, for example, a few times higher density than that of the ambient HI gas is required. We think this is quite unlikely because beams 8, 9, 15, and 16, located on local maximum of the HI loop structure, show less [C II] emission than that from beams 10 – 14.

We propose that the excess [C II] emission originates from PDRs formed around molecular clouds, where CO molecules are photodissociated by FUV photons to produce  $\text{C}^+$  ions (and  $\text{C}^0$ ) while most of the hydrogen remains in molecular form (van Dishoeck & Black 1988; Hollenbach et al. 1991). At the surface of a PDR, [C II]  $158\mu\text{m}$  line emission dominates the gas cooling, while grain photoelectric heating is dominant over almost the entire PDR. Therefore, the spatial variation of [C II] emission should match the variation of the grain photoelectric heating. According to models of Hollenbach et al. and Wolfire et al. (1995), the efficiency of grain photoelectric heating is almost constant in the case of  $G_0 \sim 1$ ,  $n(\text{H}_2) \sim 20 \text{ cm}^{-3}$  (average density of the MBM clouds, Table 2), and  $T \sim 100\text{K}$ . Thus the variation of the grain photoelectric heating rate must be due to variation of the dust-to-gas mass ratio or variation of the FUV field strength. Since the FIR continuum emission spatially well-correlated with the CO emission, the variation of dust-to-gas mass ratio is unlikely, and variation of the FUV strength is most probable.

The variation of FUV strength can be explained by the location of a FUV source and the distribution of attenuating material. Because the MBM clouds are located at about 60pc above the Galactic plane (calculated from  $D = 100\text{pc}$  and  $b \simeq 38^\circ$ ), cloud surfaces facing the Galactic plane are presumably illuminated by stronger FUV photons. Using the average density  $n(\text{H}_2) = 20 \text{ cm}^{-3}$  of the MBM clouds and the length of the molecular filament on the sky ( $\sim 10\text{pc}$ ), the optical depth through the excess [C II] emission region is estimated to be  $A_V = 0.65\text{mag}$  or  $A_{\text{FUV}} = 1.2\text{mag}$  ( $A_{\text{FUV}}/A_V = 1.8$ ; De Jong, Dalgarno, & Boland 1980). The HI gas further contributes to the attenuation. Thus, the FUV photons are significantly attenuated toward higher Galactic latitudes by the molecular and the HI clouds, resulting in weaker [C II] emission. This might be the reason why the small CO cloudlets found at higher latitude regions (in §4.3) withstand photodissociation and indeed the [C II] line to FIR continuum ratio is anomalously low. The depth of the [C II] emission

region agrees well with the theoretical thickness of the  $C^+$  region formed on the surface of a molecular cloud illuminated by the standard interstellar FUV flux ( $A_V(C^+) \sim 0.5\text{mag}$ ; van Dishoeck & Black 1988), supporting this interpretation.

#### 4.5. Overall Observational Properties of the MBM clouds

The integrated FIR continuum intensity may be calculated from the observed  $152.5\mu\text{m}$  intensity assuming the FIR spectrum determined by the other photometric channels onboard the instrument ( $T = 16.6\text{K}$  gray-body with an emissivity  $\propto \lambda^{-2}$ ; Kawada et al. 1994). By averaging the [C II] intensity and the integrated FIR continuum intensity over the CO regions (beams 8 – 14), we obtain an average ratio of  $[C\ II]/FIR \simeq 0.0071$ , which is close to the all sky average of 0.0082 reported by the FIRAS (Wright et al. 1991) which is heavily weighted toward the Galactic plane. Using the FIR continuum emissivity obtained for the HI clouds (§4.1), the observed [C II]/FIR ratio corresponds to a [CII] cooling rate of  $\Lambda_{CII} \simeq 3 \times 10^{-26} \text{ergs s}^{-1} \text{H}_{\text{nuc}}^{-1}$ , which is a factor of two larger than that of the HI clouds. This may indicate that the heating efficiency is higher in the PDRs around the molecular clouds than in the diffuse HI clouds. We also obtain an average ratio of  $[C\ II]/CO \simeq 420$  by taking the observed  $W_{CO}$  and converting to brightness by  $1\text{K km s}^{-1} = 1.6 \times 10^{-9} \text{ergs s}^{-1} \text{cm}^{-2} \text{sr}^{-1}$ . This ratio is significantly smaller than that of molecular clouds in the Galactic plane (1500; Shibai et al. 1991), as expected if  $G_0$  is lower at high Galactic latitude than on the Galactic plane (Hollenbach et al. 1991).

### 5. Summary

We report the first [C II]  $158\mu\text{m}$  line observation of high latitude molecular clouds. The [C II] line and  $152.5\mu\text{m}$  continuum data are obtained using a rocket-borne spectrophotometer which observed a region at high Galactic latitude in Ursa Major including the MBM clouds. We also present the results of a follow-up observation of the millimeter  $^{12}\text{CO } J = 1 \rightarrow 0$  line.

Over the observed region the ratio of molecular hydrogen column density to velocity-integrated CO intensity is  $X = 1.19 \pm 0.29 \times 10^{20} \text{cm}^{-2} (\text{K km s}^{-1})^{-1}$ , assuming a constant FIR emissivity per hydrogen nucleus for both the molecular and the atomic regions. We have also discovered three small CO cloudlets as a result of the  $^{12}\text{CO}$  observation of the selected region in Ursa Major. Using the factor X and the observed width of the CO line, we estimate the mass and the turbulent pressure of the CO cloudlets. We find that these

molecular cloudlets, as well as the MBM clouds, are not gravitationally bound. Magnetic pressure and turbulent pressure dominate the dynamic balance of the clouds.

After subtracting the HI and the background contributions, we compare the spatial distribution of the [C II] line, the  $152.5\mu\text{m}$  continuum, and the  $^{12}\text{CO}$  line intensity. The [C II] emission peak is displaced from the  $^{12}\text{CO}$  line intensity peak, while the  $152.5\mu\text{m}$  continuum emission is spatially correlated with the  $^{12}\text{CO}$  line emission. We discuss the origin of the [C II] emission and conclude that the [C II] emission most probably originates in PDRs around the molecular clouds illuminated by the local UV radiation field.

The average ratio of the [C II] line to the integrated FIR continuum intensity over the MBM clouds was found to be 0.0071, which is close to the all sky average of 0.0082 reported by the FIRAS on the COBE. This [C II]/FIR ratio corresponds to the [CII] cooling rate  $\Lambda_{\text{CII}} \simeq 3 \times 10^{-26} \text{ ergs s}^{-1} \text{H}_{\text{nuc}}^{-1}$ , which is a factor of two larger than that of HI clouds. The [C II]/CO ratio calculated in the same manner was 420, which is significantly lower than that of molecular clouds in the Galactic plane.

We would like to thank to all the collaborators of the S-520-15 rocket experiment: T. Matsumoto, P. L. Richards, A. E. Lange, V. V. Hristov, S. Matsuura, and P. D. Maukopf. We also thank H. Okuda and the ISAS launch staff for their kind support. We thank R. Reynolds for providing the  $\text{H}\alpha$  data toward the Ursa Major region. This work was supported by the ISAS, by the Daiko Science Foundation, by grant-in-aids (No. 03249213, 03740128, & 04233215) from the Ministry of Education, Science and Culture in Japan, and by the National Aeronautics and Space Administration under grants NAGW-1352 and NGT-50771.

## REFERENCES

- Bennett, C. L., et al. 1994, *ApJ*, 434, 587.
- Bock, J. J., et al. 1993, *ApJ*, 410, L115
- Dalgarno, A., & McCray, R. M. 1972, *ARA&A*, 10, 375
- de Vries, H. W., Heithausen, A., & Thaddeus, P. 1987, *ApJ*, 319, 723 (VHT)
- De Jong, T., Dalgarno, A., & Boland, W. 1980, *A&A*, 91, 68
- Dwek, E., et al. 1997, *ApJ*, 475, 565
- Fukui, Y., & Sakakibara, O. 1992, *Mitsubishi Electric ADVANCE*, 60, 11
- Habing, H. J. 1968, *Bull. Astron. Inst. Netherlands*, 19, 421
- Heiles, C. 1989, *ApJ*, 336, 808
- Heiles, C. & Habing, H. J. 1974, *A&AS*, 14, 1
- Hollenbach, D. J., Takahashi, T., & Tielens, A. G. G. M. 1991, *ApJ*, 377, 192
- Joncas, G., Boulanger, F. & Dewdney, P. E. 1992, *ApJ*, 397, 165
- Kawada, M., et al. 1994, *ApJ*, 425, L89
- Magnani, L., Blitz, L., & Mundy, L. 1985, *ApJ*, 295, 402 (MBM)
- Matsuhara, H., et al. 1994, *PASJ*, 46, 665
- Matsuura, S. et al. 1994, *PASP*, 106, 770
- Penprase, B. E. 1993, *ApJS*, 88, 433
- Reynolds, R. J. 1992, *ApJ*, 392, L35
- Reynolds, R. J. 1993, in *Back to the Galaxy*, eds S. S. Holt & F. Verter (*AIP Conf. Proc.* 278), 303
- Shibai, H., et al. 1991, *ApJ*, 374, 522
- Spitzer, L. 1978, *Physical Processes in the Interstellar Medium* (New York: Wiley)
- Tielens, A. G. G. M., & Hollenbach, D. 1985, *ApJ*, 291, 722.

van Dishoeck, E. F., & Black, J. H. 1988, *ApJ*, 334, 771

Wheelock, S., et al. 1994, *IRAS Sky Survey Atlas Explanatory Supplement*, JPL Publication 94-11 (Pasadena: JPL)

Wolfire, M. G., Hollenbach, D., McKee, C. F., Tielens, A. G. G. M., & Bakes, E. L. 1995, *ApJ*, 443, 152

Wright, E. L., et al. 1991, *ApJ*, 381, 200

Fig. 1.— Rocket-borne [C II] and FIR continuum observations were performed along a triangular path crossing the high latitude molecular clouds(MBM 27/28/29/30) in Ursa Major. The contour map of the MBM clouds is from VHT. For beams shown by the circles,  $^{12}\text{CO } J = 1 \rightarrow 0$  data are also available. Beams shown by filled circles are mapped with the 4m millimeter telescope at Nagoya University. Size of the circles corresponds to the beam size of the rocket observation.

Fig. 2.— (a)  $152.5\mu\text{m}$  continuum intensity vs. atomic hydrogen column density( $N_{\text{HI}}$ ), and (b) [C II]  $158\mu\text{m}$  line intensity vs.  $N_{\text{HI}}$ . For most of the beam positions with  $N_{\text{HI}} < 2 \times 10^{20} \text{ cm}^{-2}$ , no CO data are available. From the correlation over beams with  $N_{\text{HI}} < 2 \times 10^{20} \text{ cm}^{-2}$  and beams where we confirmed there is no significant CO emission(beams 2, 4, 5, 6, 7, 15, 16, where  $W_{\text{CO}} < 0.2\text{K km s}^{-1}$ ), we obtain the average FIR continuum emissivity and the [C II] cooling rate of the HI regions(solid lines).

Fig. 3.—  $^{12}\text{CO } J = 1 \rightarrow 0$  contour maps obtained with the 4m millimeter telescope at Nagoya University, superposed on IRAS  $100\mu\text{m}$  maps. Eight beams(filled circles in Fig. 1) were surveyed for CO emission(typically  $40' \times 40'$ ,  $2' - 8'$  grids) with positive detection for the five beams shown here. The contours are spaced at  $\Delta W_{\text{CO}} = 0.6\text{K km s}^{-1}$  for beams 3, 8, 9 and  $0.4\text{K km s}^{-1}$  for beams 4, 5. The lowest contour level is  $0.6\text{K km s}^{-1}$ .

Fig. 4.— Typical  $^{12}\text{CO } J = 1 \rightarrow 0$  spectra for beams 3, 4, and 5, showing the newly discovered small molecular cloudlets. (a) Spectra at  $(\Delta\alpha, \Delta\delta)=(-6, -6)$  and  $(-22, -2)$  in Fig. 3a, (b) spectrum at  $(+2, +6)$  in Fig. 3b, (c) spectrum at  $(-2, +10)$  in Fig. 3c.

Fig. 5.— Excess(corrected for HI and background contributions)  $152.5\mu\text{m}$  continuum emission vs.  $W_{\text{CO}}$ . The best linear fit is shown by the dashed line.

Fig. 6.— (a) Spatial distribution of  $W_{\text{CO}}$ (filled triangles) and excess [C II] line intensity(filled circles) for beams 2 – 14 shown in (b) a part of the observed region. The upper limits of  $W_{\text{CO}}$  are  $3\sigma$ .